IEEE Photonics Journal
An IEEE Photonics Society Publication

Open Access

Simultaneous Suppression of Even-Order and Third-Order Distortions in Directly Modulated Analog Photonic Links

Volume 9, Number 3, June 2017

Yao Ye
Lei Deng
Shichao Chen
Mengfan Cheng
Ming Tang, *Senior Member, IEEE*
Songnian Fu
Minming Zhang
Di Zhang
Benxiong Huang
Deming Liu

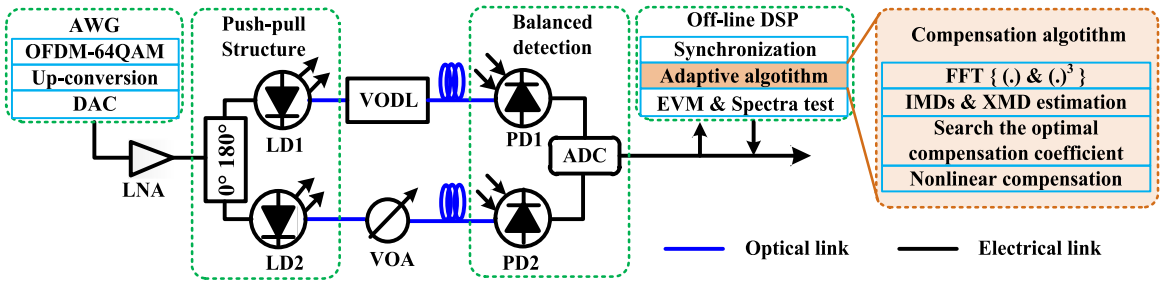

DOI: 10.1109/JPHOT.2017.2700048
1943-0655 © 2017 IEEE

IEEE photonics SOCIETY

IEEE

Simultaneous Suppression of Even-Order and Third-Order Distortions in Directly Modulated Analog Photonic Links

Yao Ye,[1] Lei Deng,[2] Shichao Chen,[2] Mengfan Cheng,[2] Ming Tang,[2] *Senior Member, IEEE*, Songnian Fu,[2] Minming Zhang,[2] Di Zhang,[1] Benxiong Huang,[1] and Deming Liu[2]

[1]School of Electronic Information and Communications, Huazhong University of Science and Technology, Wuhan 430074, China
[2]Next Generation Internet Access National Engineering Laboratory, School of Optical and Electronic Information, Huazhong University of Science and Technology, Wuhan 430074, China

DOI:10.1109/JPHOT.2017.2700048

Manuscript received March 15, 2017; revised April 18, 2017; accepted April 27, 2017. Date of publication May 2, 2017; date of current version May 17, 2017. This work was supported in part by the National "863" Program of China under Grant 2015AA016904 and in part by the National Nature Science Foundation of China under Grant 61675083, Grant 61331010, and Grant 61505061. Corresponding author: Lei Deng (e-mail: denglei_hust@mail.hust.edu.cn).

Abstract: A high-linearity directly-modulated analog photonic link (APL) with simultaneous suppression of the even-order intermodulation distortion, third-order intermodulation distortion (IMD3), and cross-modulation distortion (XMD) is proposed and experimentally demonstrated by the corporation of push–pull structure and an adaptive compensation algorithm. In the proposed directly-modulated APL system, the push–pull structure is introduced to effectively eliminate all the even-order nonlinear distortions, including the second-order intermodulation distortion and the second-order harmonic distortions. To further simultaneously suppress the IMD3 and XMD, an adaptive compensation algorithm is designed and adopted at the receiver. The experimental results show that the second-order spurious-free dynamic range and the third-order spurious-free dynamic range is improved by 19.8 and 12.4 dB, respectively, corresponding to 7.15% error vector magnitude performance improvement for a 120 Mb/s 64QAM-OFDM RF signal transmission when the input RF power is 13 dBm.

Index Terms: Radio over fiber (RoF), fiber optics link and subsystems, digital signal processing.

1. Introduction

To data, the analog photonic link (APL) has attracted increasing attention due to the fact that it takes advantage of both fiber optics and radio-wave communication systems such as broad bandwidth, low insertion loss, and resistance to electromagnetic interference [1]–[3]. In APLs, spurious-free dynamic range (SFDR) is a main figure of merit which is mainly limited by the nonlinear distortions including the second-order inter-modulation distortions (IMD2), the second-order harmonic distortions (HD2), the third-order inter-modulation distortions (IMD3) and the cross-modulation distortions (XMD) induced by the electrical-to-optical (E/O) and optical-to-electrical (O/E) conversion [4]–[6]. In particular, in some applications such as radio-over-fiber (RoF) systems,

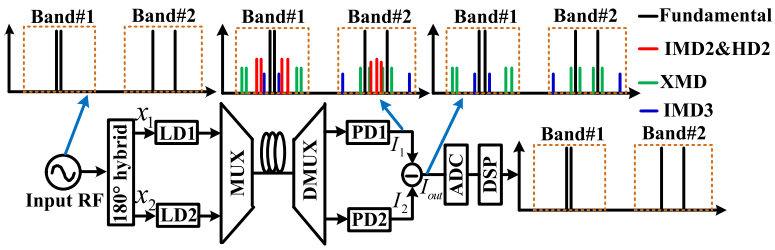

Fig. 1. Schematic diagram of the proposed technique and the electrical spectra of the received RF signal.

phased-array radars, and radio astronomy [7], stringent SFDR requirements are imposed. To address these issues, various techniques for SFDR enhancement in APLs have been investigated, such as pre-distortion [8], [9], optical spectrum processing [10], [11], post digital linearization [12], and dual-polarization modulator [13]. All the techniques mentioned above could eliminate the IMD3 effectively, but the IMD2 is less concerned. However, the IMD2 and HD2 is the main factor limiting the multi-octave dynamic range, and some applications like antenna remoting and high speed radio over fiber systems often demand a high SFDR over a multi-octave dynamic range [14]. Although the IMD2 could be also eliminated by using the techniques in [15]–[19], and even the IMD2 and IMD3 could be simultaneously suppressed in [20], all these methods are focusing on externally-modulated APLs based on Mach-Zehnder modulator (MZM) rather than directly-modulated ones.

However, compared with the externally-modulated APLs, the directly-modulated APLs are more attractive in the cost-sensitive scenarios such as interconnecting large arrays and medium reach applications due to their lower power budget, smaller size and simpler operation [21]–[23]. Therefore, linearity improvement methods which could be applied to directly-modulated APLs are highly desired. Unfortunately, unlike the MZM-based APLs, the DML-based APL can't eliminate IMD2 and HD2 just by using the quadrature bias point. Therefore, to achieve multi-octave, high-linearity and cost-efficient APLs, the linearity technologies which could suppress IMD2, HD2, IMD3, and XMD simultaneously for DML-based APL become urgent needs. In our previous work, we propose a method based on the corporation of push-pull structure and digital signal process (DSP) algorithm to enhance the SFDR2 and SFDR3 performance of the DML-based APL [24]. However, the proposed DSP algorithm need to have prior knowledge of many modulation parameters, and all these modulation parameters will be varied when the input RF power changes in practice, which makes this DSP algorithm complex.

In this paper, to simultaneously suppress IMD2, HD2, IMD3, and XMD, a novel method based on the corporation of a push-pull structure and an adaptive compensation algorithm is proposed in the directly-modulated APL. All the even-order nonlinear distortions (including IMD2, HD2 and IMD4) can be effectively eliminated in virtue of the push-pull manner with two complementary outputs and a balanced detection at the receiver. Moreover, an adaptive compensation algorithm is designed to eliminate the IMD3 and XMD after the balanced detection. By this way, a high linearity directly-modulated APL could be achieved. The experimental results show that the IMD2, HD2, IMD3 and XMD of the directly-modulated APL are simultaneously suppressed, corresponding to 7.15% EVM performance improvement for the used 120 Mb/s 64QAM-OFDM RF signal when the input RF power is 13 dBm. Furthermore, the SFDR2 and SFDR3 are improved by 19.8 dB and 12.4 dB, respectively.

2. Operation Principle

The schematic diagram of the proposed corporation of push-pull structure and DSP algorithm is shown in Fig. 1. In some practical multi-octave APLs, the IMD2, HD2, IMD3, and XMD induced by nonlinear E/O and O/E conversion are located in the fundamentals bands, and it is impossible to filter them out by using electrical filter. All these nonlinear distortion components will significantly

degrade the transmission performance of the directly-modulated APLs. To achieve a high linearity APL, all these nonlinear distortions should be eliminated simultaneously.

2.1 Even-Order Distortions Suppression by Push–Pull Manner

As shown in Fig. 1, the input RF signal with two center angular frequencies w_1 and w_2 can be expressed as

$$x(t) = A_0\left[cos(w_1 t)\cdot\sum_{k=1}^{N} cos(k\delta_1 t) + cos(w_2 t)\cdot\sum_{k=1}^{N} cos(k\delta_2 t)\right] \tag{1}$$

where A_0 is the amplitude of the input RF signals, δ_1 and δ_2 are the frequency interval of the two pairs of the input RF signals, N is number of the tones of each group RF signal, and k is a positive integer less than N. The input RF signal is then divided into two parts $x_1(t)$ and $x_2(t)$ by an electrical 180°hybrid. The generated RF signals in the upper and lower arms can be expressed as

$$\begin{pmatrix} x_1(t) \\ x_2(t) \end{pmatrix} = \frac{1}{\sqrt{2}}\begin{pmatrix} 1 & 0 \\ 0 & e^{j\pi} \end{pmatrix}\begin{pmatrix} x(t) \\ x(t) \end{pmatrix}. \tag{2}$$

These two RF signals are used to modulate the first laser diode (LD1) and the second laser diode (LD2) in a push-pull manner. After fiber transmission and balanced photodetection by the first photodiode (PD1) and the second photodiode (PD2), the received RF signals $I_1(t)$ and $I_2(t)$ in the upper and lower arms can be described as

$$\begin{pmatrix} I_1(t) \\ I_2(t) \end{pmatrix} = \begin{pmatrix} \alpha_1 & 0 \\ 0 & \alpha_2 \end{pmatrix}\begin{pmatrix} \eta_1 & 0 \\ 0 & \eta_2 \end{pmatrix}\begin{pmatrix} I_{b1} + m_1\sum_{n=1}^{\infty}[a_n {x_1}^n(t)] \\ I_{b2} + m_2\sum_{n=1}^{\infty}[b_n {x_2}^n(t)] \end{pmatrix} \tag{3}$$

where α_1 and α_2 are the link attenuation coefficients in the two arms of the APL, η_1 and η_2 are the responsivity of PD1 and PD2, respectively. I_{b1} and I_{b2} are the bias currents of LD1 and LD2, m_1 and m_2 are the electrical modulation index, and a_n ($n = 1, 2, 3\ldots$) and b_n ($n = 1, 2, 3\ldots$) are the n-order nonlinear coefficients of the transfer function of upper and lower link, respectively. Subsequently, the received signal in the upper arm is subtracted by that in the lower arm, and the generated RF signal $I_{out}(t)$ can be described as

$$\begin{aligned} I_{out} &= I_1(t) - I_2(t) \\ &= (\alpha_1\eta_1 I_{b1} - \alpha_2\eta_2 I_{b2}) + \sum_{n=1}^{\infty}\left\{\left(\frac{1}{\sqrt{2}}\right)^n\left(m_1\alpha_1\eta_1 a_n - m_2\alpha_2\eta_2 b_n e^{jn\pi}\right)x^n(t)\right\} \end{aligned} \tag{4}$$

where $x^n(t)$ can be expanded by using the binomial theorem and expressed as

$$\begin{aligned} x^n(t) &= A_0^n\left[cos(w_1 t)\cdot\sum_{k=1}^{N} cos(k\delta_1 t) + cos(w_2 t)\cdot\sum_{k=1}^{N} cos(k\delta_2 t)\right]^n \\ &= A_0^n\sum_{r=0}^{n} C_n^r[cos(w_1 t)\cdot\sum_{k=1}^{N} cos(k\delta_1 t)]^r\cdot[cos(w_2 t)\cdot\sum_{k=1}^{N} cos(k\delta_2 t)]^{n-r}. \end{aligned} \tag{5}$$

As we know, $\cos^{\beta}(wt)$ can be expanded by using Euler's formula and binomial theorem and represented as

$$\cos^{\beta}(wt) = \left[\frac{1}{2}(e^{jwt} + e^{-iwt})\right]^{\beta} = \left(\frac{1}{2}\right)^{\beta}\sum_{\gamma=0}^{\beta} C_{\beta}^{\gamma} e^{j(2\gamma-\beta)wt}. \tag{6}$$

TABLE 1
Major Output Components of $x^n(t)$ When n Is Odd or Even ($N = 1$)

n is odd					
γ is odd		(n-γ) is even		Output RF signals	
$\cos^{\gamma}(w_1 t)$	$\cos^{\gamma}(\delta_1 t)$	$\cos^{(n-\gamma)}(w_2 t)$	$\cos^{(n-\gamma)}(\delta_2 t)$	$x^n(t)$	Derivation
w_1	δ_1	$0 \times w_2$	$0 \times \delta_2$	$w_1 \pm \delta_1$	Fundamental signal
w_1	$3\delta_1$	$0 \times w_2$	$0 \times \delta_2$	$w_1 \pm 3\delta_1$	IMD3
w_1	δ_1	$0 \times w_2$	$2\delta_2$	$(w_1 \pm \delta_1) \pm 2\delta_2$	XMD
...	...	...	...	...	...
γ is even		(n-γ) is odd		Output RF signals	
$\cos^{\gamma}(w_1 t)$	$\cos^{\gamma}(\delta_1 t)$	$\cos^{(n-\gamma)}(w_2 t)$	$\cos^{(n-\gamma)}(\delta_2 t)$	$x^n(t)$	Derivation
$0 \times w_1$	$0 \times \delta_1$	w_2	δ_2	$w_2 \pm \delta_2$	Fundamental signal
$0 \times w_1$	$0 \times \delta_1$	w_2	$3\delta_2$	$w_2 \pm 3\delta_2$	IMD3
$0 \times w_1$	$2\delta_1$	w_2	δ_2	$(w_2 \pm \delta_2) \pm 2\delta_1$	XMD
...	...	...	...	...	...
n is even					
γ is odd		(n-γ) is odd		Output RF signals	
$\cos^{\gamma}(w_1 t)$	$\cos^{\gamma}(\delta_1 t)$	$\cos^{(n-\gamma)}(w_2 t)$	$\cos^{(n-\gamma)}(\delta_2 t)$	$x^n(t)$	Derivation
w_1	δ_1	w_2	δ_2	$(w_2 \pm \delta_2) - (w_1 \pm \delta_1)$	IMD2
$3w_1$	$3\delta_1$	w_2	δ_2	$3(w_1 \pm \delta_1) - (w_2 \pm \delta_2)$	IMD4
w_1	$3\delta_1$	w_2	δ_2	$(w_1 \pm 3\delta_1) \pm (w_2 \pm \delta_2)$	IMD2
...	...	...	...	...	...
γ is even		(n-γ) is even		Output RF signals	
$\cos^{\gamma}(w_1 t)$	$\cos^{\gamma}(\delta_1 t)$	$\cos^{(n-\gamma)}(w_2 t)$	$\cos^{(n-\gamma)}(\delta_2 t)$	$x^n(t)$	Derivation
$0 \times w_1$	$0 \times \delta_1$	$2w_2$	$2\delta_2$	$2(w_2 \pm \delta_2)$	HD2
$2w_1$	$2\delta_1$	$0 \times w_2$	$0 \times \delta_2$	$2(w_1 \pm \delta_1)$	HD2
$2w_1$	$0 \times \delta_1$	$0 \times w_2$	$0 \times \delta_2$	$2w_1$	IMD2
...	...	...	...	...	...

As shown in (6), if β is even, 2γ-β is even. It could be clearly observed that the expansion of $\cos^{\beta}(wt)$ only contain $\cos(|2\gamma\text{-}\beta|wt)$, where $|2\gamma - \beta| = 0, 2, 4 \ldots$. Similarly, if β is odd, the expansion of $\cos^{\beta}(wt)$ only contain $\cos(|2\gamma\text{-}\beta|wt)$, where $|2\gamma - \beta| = 1, 3, 5 \ldots$.Therefore, from (5) and (6), a conclusion can be drawn that $x^n(t)$ can only induces all the even-order distortions (including IMD2, HD2, IMD4 and HD4) when n is even. Similarly, $x^n(t)$ can only induces all the odd-order distortions (including IMD3 and IMD5) when n is odd. To explain more clearly, Table 1 gives the major output components of $x^n(t)$ when $N = 1$, such as fundamental components ($w_1 \pm \delta_1, w_2 \pm \delta_2$),

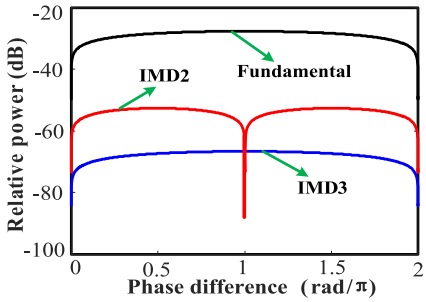

Fig. 2. Simulated relative power of the received RF signal as a function of the phase difference.

IMD2 components ($2w_1$, $(w_2 \pm \delta_2) - (w_1 \pm \delta_1)$), HD2 components ($2(w_1 \pm \delta_1)$, $2(w_2 \pm \delta_2)$), IMD3 components ($w_1 \pm 3\delta_1$, $w_2 \pm 3\delta_2$) and XMD components ($(w_1 \pm \delta_1) \pm 2\delta_2$, $(w_2 \pm \delta_2) \pm 2\delta_1$).

We can appropriately adjust the parameters of α_1, α_2, m_1 and m_2 to make $m_1\alpha_1\eta_1 a_n = m_2\alpha_2\eta_2 b_n$, and the DC component in (4) can be filtered out by a filter. Therefore, (4) can be rewritten as

$$I_{out} = 2m_1\alpha_1\eta_1 \sum_{n=1}^{\infty} \left\{ \left(\frac{1}{\sqrt{2}} \right)^{2n-1} a_{2n-1} x^{2n-1}(t) \right\}. \tag{7}$$

Equation (7) shows that $x^{2n}(t)$ are eliminated, and that means all the even-order distortion components (including IMD2 and HD2) which are the main factors limiting the multi-octave dynamic range can be completely suppressed. However, the power of the received odd-order distortion components (including the fundamental, IMD3 and XMD) will be increased by 6 dB compared with the conventional single-arm APL. This indicates that the residual IMD3 and XMD become the main factors to limit the system performance.

To investigate the impact of the phase difference between the upper and low arms on the linear performance of APL when N = 1. Two groups of two-tone RF signal with center frequencies of 2.4 GHz and 3.2 GHz and frequency interval of 10 MHz are used in our simulation. The relative power of the received RF signals including fundamental components, IMD2 and IMD3 components as a function of phase difference is simulated by using VPI Transmission Maker 9.0 and Matlab and plotted in Fig. 2. It could be clearly observed that the phase difference of the output signals at the upper and lower arms are required to be π to completely eliminate the even-order distortion components.

2.2 IMD3 and XMD Suppression by the Adaptive Algorithm

To further eliminate the IMD3 components, a DSP algorithm is proposed in our previous work [24], but the parameters setting in that algorithm is relative to the amplitude and nonlinear coefficients of the transfer function of APL, which makes that algorithm quite complex.

To solve this problem, it is necessary to optimize the post-compensation algorithm and make it more simple and effective. Obviously, the nonlinearity of APL only depends on the odd terms of $x(t)$ as shown in (7). Therefore, we can construct an odd compensation function in digital domain to counteract the original nonlinear distortion components, and this compensation function can be expressed as

$$y_{out} = I_{out} - C_3 {I^3}_{out} \tag{8}$$

where C_3 is the compensation coefficient. Substituting (7) to (8), (8) can be rewritten as

$$y_{out} = \sqrt{2}\lambda a_1 x(t) + \left(\frac{\sqrt{2}}{2}\lambda a_3 - 2\sqrt{2}C_3\lambda^3 {a_1}^3 \right) x^3(t) + \left(\frac{\sqrt{2}}{4}\lambda a_5 - 3\sqrt{2}C_3\lambda^3 {a_1}^2 a_3 \right) x^5(t) \tag{9}$$

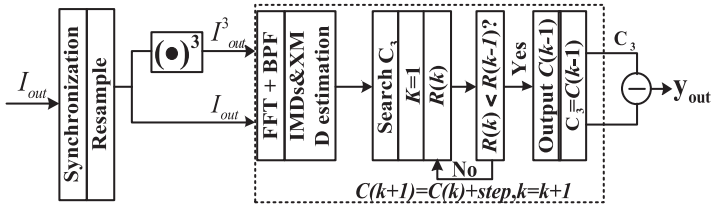

Fig. 3. Detailed flowchart of the proposed adaptive algorithm.

where $\lambda = m_1\alpha_1\eta_1$. Note that y_{out} only contain odd teams of $x(t)$, which indicates there are no even-order distortion components existing. Higher order than five of $x(t)$ could be ignored due to their negligible contribution to nonlinear distortions. As mentioned in Section 2.1, both $x^3(t)$ and $x^5(t)$ can induce IMD3 and XMD, and $x^5(t)$ can also induce IMD5. According to (8), the perfect linearization conditions would be achieved when

$$\begin{cases} \frac{\sqrt{2}}{2}\lambda a_3 - 2\sqrt{2}C_3\lambda^3 {a_1}^3 = 0 \\ \frac{\sqrt{2}}{4}\lambda a_5 - 3\sqrt{2}C_3\lambda^3 {a_1}^2 a_3 = 0 \end{cases} \tag{10}$$

is satisfied.

Unfortunately, such conditions cannot be satisfied simultaneously by just adjusting the parameters of m_1, α_1, and η_1 in APL. Therefore, it's necessary to search the optimal compensation coefficient C_3 to make compromises between them. However, the value of m_1 is time-varying due to the drift of bias voltage. Moreover, these related parameters will be changed when the central frequency of the input RF signal is different, which indicates that the compensation coefficient C_3 should be adjusted dynamically to accommodate the practical scenario. To overcome these challenges, a self-adaptive algorithm to adapt the changing parameters of APL is highly required. By introducing the definition of fundamental signal to the distortion components (IMD3, XMD and IMD5) ratio (R), and choosing the optimal operating point to make R maximal, the optimum conditions for simultaneous suppressions of IMD3 and XMD can be satisfied. R can be described as

$$R = \min \begin{Bmatrix} R_{(IMD3)} = 10\lg(P_F/P_{IMD3}), \\ R_{(XMD)} = 10\lg(P_F/P_{XMD}), \\ R_{(IMD5)} = 10\lg(P_F/P_{IMD5}) \end{Bmatrix} \tag{11}$$

where P_F, P_{IMD3}, P_{XMD}, and P_{IMD5} are the power of the fundamental signal, IMD3, XMD, and IMD5 in y_{out}, respectively. The details of the proposed adaptive algorithm which could be used to search the optimal compensation coefficient C_3 is shown in Fig. 3.

Obviously, the frequency spectrum of the received RF signal I_{out} and its cubic term I^3_{out} could be obtained by using fast Fourier transform (FFT) and band-pass filter (BPF). Subsequently, the optimal value of the compensation coefficient C_3 is searched as follows. First, the frequency spectrum position of the fundamental signals, IMD3 and XMD signals is obtained according to the known center frequency and bandwidth of the input RF signal, and then the IMD3 and XMD power of both I_{out} and I^3_{out} could be achieved. The maximal value of R is defined as the judgment basis for the best nonlinear compensation. If the $R(k)$ is not maximal, the compensation coefficient $C(k)$ is updated with a constant step-size. Otherwise, the coefficient $C(k\text{-}1)$ can be considered as the optimized value. At last, the compensation coefficient C_3 is equal to $C(k\text{-}1)$ and the IMD3, XMD and IMD5 of APL could be suppressed simultaneously.

It should be noted that in the proposed algorithm, only two FFT operations and an iteration process is required, which makes the algorithm complexity relatively low. Moreover, only the center frequency and the bandwidth of the input RF signals rather than all the parameters of APL links are needed to know beforehand at the receiver. Furthermore, the value of the optimal coefficient C_3 could be adjusted dynamically to the practical situation, which makes the proposed algorithm practical.

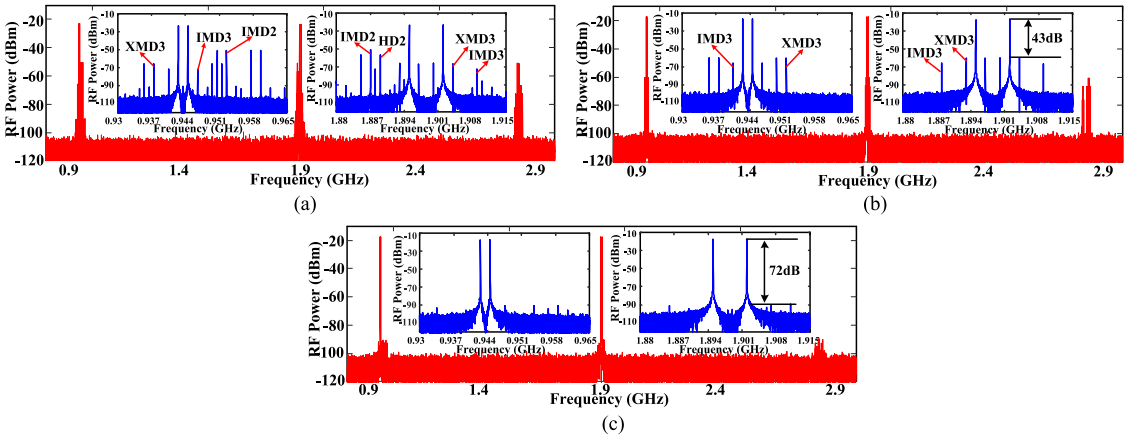

Fig. 4. Electrical spectra of the output RF signals in traditional single-arm APLs (a), APLs only using the push-pull structure (b), and APLs using the proposed method (c).

3. Simulation Results and Analysis

For the multi-octave applications, not only the IMD3 and XMD but also the IMD2 and HD2 will lie in the spectral range of interest. For example, the effective communication band of GMS900 is 930 MHz-954 MHz, and one of the communication band of TD-LTE is 1880 MHz-1900 MHz which is chosen by China Mobile Communications Corporation (CMCC). Obviously, the generated IMD2 components of the downstream signal of GMS900 will disturb the TD-LTE RF signal. To evaluate the feasibility of the proposed scheme, a simulation setup based on Matlab has been built up, and two groups of two-tone RF signals with central frequency of $f_1 = 0.94$ GHz and $f_2 = 1.896$ GHz are used. In our simulation, the nonlinearity performance of the traditional directly-modulated APLs, APLs only with the push-pull structure, and APLs using the proposed method are tested comparatively.

Fig. 4 shows the measured electrical spectra of the output RF signals in these three cases. As shown in Fig. 4(a), considerable IMD2, HD2, IMD3 and XMD are clearly observed in the traditional directly-modulated APLs due to the nonlinear transfer function. When the push-pull structure is adopt in APLs, the IMD2 and HD2 are significantly suppressed in Fig. 4(b). However, the IMD3 and XMD around the fundamental components are improved by 6 dB of the push-pull structure compared to the single-arm. When the push-pull structure is used by the corporation of the proposed adaptive DSP algorithm, the fundamental to the modulated distortions power ratio is improved from 43 dB to 72 dB as shown in Fig. 4(c), and all these nonlinear distortion components are simultaneously suppressed.

According to the theoretical analysis in Section 2 and the result of simulation, it should be noted that the push-pull structure and the adaptive compensation algorithm aren't simple patch-works in our scheme. If only the push-pull structure is applied without the adaptive compensation algorithm, only even-order distortion components could be suppressed. In that case, the IMD3 and XMD will become the main factors to degrade the linearity of the APLs. Similarly, if only DSP post-compensation operation is used without push-pull structure, the complexity of the DSP algorithm will be significantly increased and the IMD2, HD2, IMD3, and XMD could not be eliminated simultaneously. Therefore, the push-pull structure could not only eliminate all the even-order distortions, but also effectively reduce the complexity of the required DSP algorithm for the IMD3 and XMD suppression. Moreover, the proposed DSP algorithm can eliminate the residual IMD3 and XMD effectively and will not introduce new even-order distortion components.

4. Experimental Setup and Results

The experimental setup of the proposed scheme is shown in Fig. 5. 120 Mb/s 64QAM-OFDM RF signal with 20 MHz bandwidth is generated in a 10 GSa/s arbitrary waveform generator (AWG,

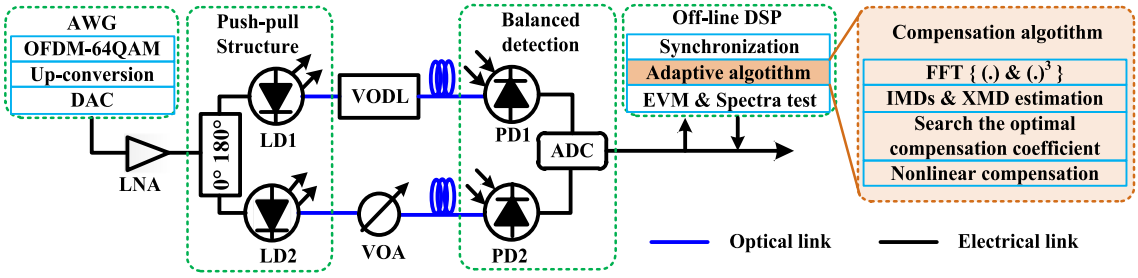

Fig. 5. Experimental setup of the proposed push-pull structure and digital signal post-compensation APL.

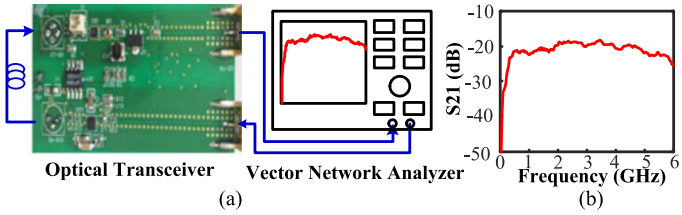

Fig. 6. Structure and the measured S21 curve of the designed optical transceiver module.

TekAWG7122B), and then be used to modulate two directly-modulated lasers ($\lambda_1 = 1309.96$ nm and $\lambda_2 = 1310.16$ nm) in a pull-push manner by using an electrical 180 degree hybrid. The variable optical attenuator (VOA) and the variable optical delay line (VODL) are adopted to realize perfect amplitude and phase matching. After 2 km fiber transmission and balanced photodetection (BPD), the 64QAM-OFDM RF signal is captured by a 25 GSa/s digital sampling oscilloscope (DSO, Tektronix DPO72504DX). Actually, to avoid the painstaking procedure of matching the length of the two arms, we can use wavelength division multiplexer and de-multiplexer to combine and separate the antiphase optical signals. Moreover, the multi-core and few-mode fiber can also be used to achieve two same length optical links. At last, offline digital signal processing including the proposed adaptive compensation algorithm and error vector magnitude (EVM) calculating is performed in the receiver, and the detail of the proposed adaptive compensation algorithm is shown in the inset of Fig. 5.

The photograph of the used optical transceiver module, which we designed, is shown in Fig. 6(a). This module includes laser driver, DFB lasers, photo-detectors, and electrical amplifiers with its size of 6.5 cm $\times$ 4.5 cm, and its price is less than $ 145. The S-parameter measurement of the used optical transceiver is carried out using a vector network analyzer (VNA, R&S@ZVL). The output reflection result is plotted in Fig. 6(b), and the 3 dB bandwidth is about 5.5 GHz (from 0.5 GHz to 6 GHz). The signal gain value is relative low below 0.5 GHz due to the high-pass characteristics of the electrical amplifier.

To investigate the impact of IMD2 and HD2, both the traditional APL and APL using the push-pull structure are tested. In our experiment, the central frequency of two input 64QAM-OFDM signals f_1 and f_2 are set to 1.6 GHz and 3.2 GHz respectively for evaluating the interference of the induced IMD2 and HD2 components of f_1 with f_2. For a comparison, another group 64QAM-OFDM signals f_3 and f_4 with central frequency of 1.4 GHz and 3.2 GHz are also used for the traditional APL, and in this case f_4 will not be disturbed by the generated IMD2 and HD2 of f_3. In all test, the EVM performance of the received 64QAM-OFDM with the central frequency of 3.2 GHz are calculated. It could be clearly observed in Fig. 7(a) that in the traditional APL, the induced of IMD2 and HD2 of f_1 will seriously degrade the EVM performance of f_2. However, by using the push-pull structure, the IMD2 and HD2 could be effectively suppressed, and 2.31% EVM performance improvement could be achieved when the input RF power is 13 dBm. The received constellations of f_2 are

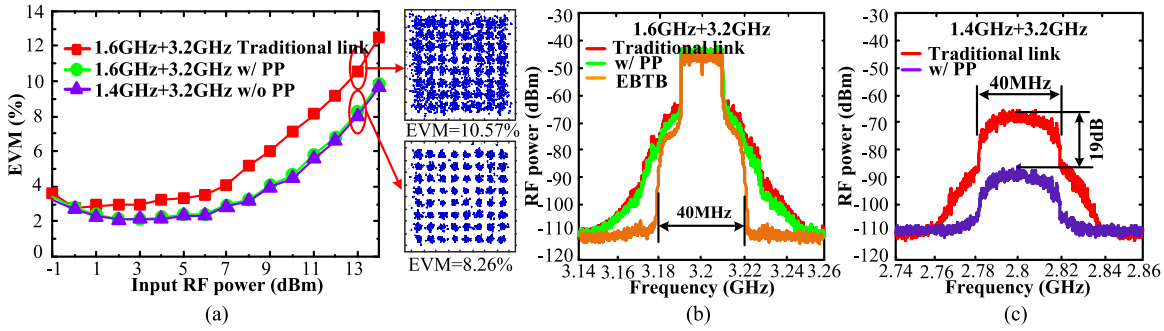

Fig. 7. Measured EVM performance (a), electrical spectra of f_2 (b) and $2f_3$ (c) in the traditional APL (Traditional link), APL using the push-pull structure (w/ PP), and the electrical back to back case (EBTB).

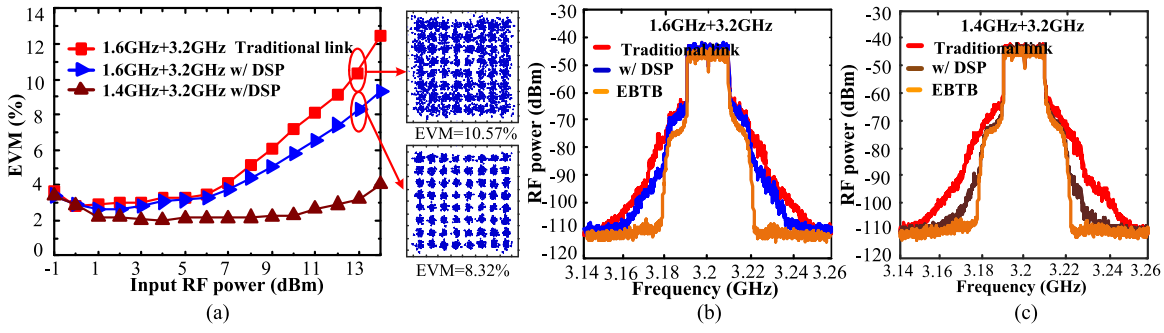

Fig. 8. Measured EVM performance (a) and electrical spectra of f_2 (b) and f_4 (c) in the traditional APL (Traditional link), the APL using the proposed DSP algorithm (w/ DSP), and the EBTB.

indicated in the insets of Fig. 7(a). Moreover, negligible power penalty could be observed between the traditional APL (with $f_3 = 1.4$ GHz and $f_4 = 3.2$ GHz) and the APL using the push-pull structure (with $f_1 = 1.6$ GHz and $f_2 = 3.2$ GHz), and it means push-pull structure cannot help to eliminate the IMD3 and XMD. Fig. 7(c) shows the even-order distortion component (with $f_3 = 1.4$ GHz and $f_4 = 3.2$ GHz) around 2.8GHz is suppressed by 19 dB by using push-pull structure. Note that in the Fig. 7(b) the electrical spectra (with $f_1 = 1.6$ GHz and $f_2 = 3.2$ GHz) without considerable improvement due to the IMD2 and HD2 of f_1 are covered by f_2 and its side lobe.

To verify the feasibility of the designed adaptive DSP post-compensation algorithm, both the traditional APL and the APL using the designed DSP algorithm are tested. Similarly, the central frequency of two input 64QAM-OFDM signals f_1 and f_2 are set to 1.6 GHz and 3.2 GHz respectively. For a comparison, another group 64QAM-OFDM signals f_3 and f_4 with central frequency of 1.4 GHz and 3.2 GHz are also used for the traditional APL, and in this case f_4 will not be disturbed by the generated IMD2 and HD2 of f_3. In all test, the EVM performance of the received 64QAM-OFDM with the central frequency of 3.2 GHz are calculated. As shown in Fig. 8(a), the measured EVM performance of f_2 become worse when the input RF power is higher than 5 dBm due to the induced IMD3 and XMD in the traditional APL. By using the designed DSP algorithm, the generated IMD3 and XMD could be suppressed, and 2.25% EVM performance improvement could be achieved when the input RF power is 13 dBm. The same phenomenon can be noted in Fig. 8(b) that the performance electrical spectra around 3.2 GHz is improved by using the proposed DSP algorithm. The received constellations of f_2 are indicated in the insets of Fig. 8(a). When $f_3 = 1.4$ GHz and $f_4 = 3.2$ GHz, as shown in Fig. 8(a) and (c) the even-order distortions induced by f_3 cannot disturb f_4, so the measured EVM performance of f_4 is improved significantly by using the proposed DSP algorithm.

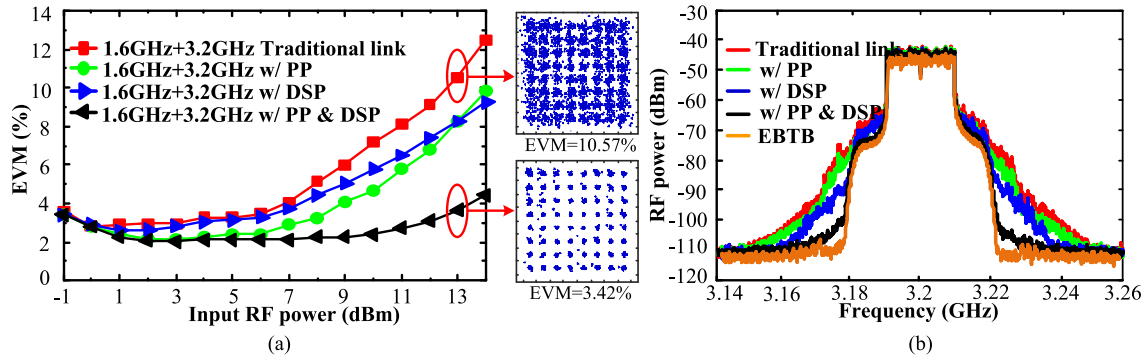

Fig. 9. Measured EVM performance (a) and electrical spectra of f_2 (b) in the traditional APL (Traditional link), the APL only with push-pull structure (w/ PP), the APL only with the designed DSP algorithm (w/ DSP), the APL with the proposed scheme (w/ PP & DSP), and the EBTB.

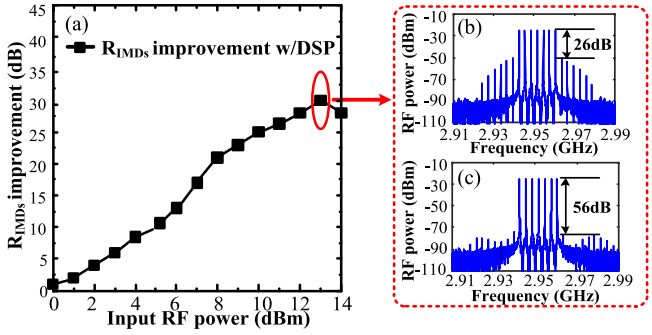

Fig. 10. (a) Measured R_{IMDs} improvement by using the proposed DSP algorithm (w/ DSP) and the electrical spectra of the received 7-tone RF signal before (b) and after (c) using the proposed DSP algorithm when the input RF power is 13 dBm.

To clearly indicate the key role of the proposed scheme, the EVM performance comparison of f_2 in the traditional APL, the APL only with push-pull structure, the APL only with the designed DSP algorithm and the APL with the proposed scheme are presented in Fig. 9(a). As mentioned above, the induced IMD2 and HD2 of f_1 is effectively suppressed if push-pull structure is used, and the induced IMD3 and XMD of f_2 can also be eliminated if the designed DSP algorithm is adopted. However, the corporation of a push-pull structure and an adaptive DSP post-compensation algorithm could help to simultaneously suppress all these nonlinear distortion components in directly-modulated APL, and it is proved in Fig. 9(a) that the measured EVM performance of f_2 is further improved to 3.42%, corresponding to 7.15% EVM performance improvement when the input RF power is 13 dBm. Similarly, the performance of the electrical spectra is improved and closely approximate to the original signal by using the proposed scheme as shown in Fig. 9(b). Moreover, from Fig. 9(a) we can conclude that IMD2 and HD2 are the main factors limiting the system performance when the input RF power is relative low, but when the input RF power is higher than 13 dBm, the IMD3 and XMD will play a major role.

To evaluate that the required parameters of the proposed DSP compensation algorithm are only the center frequency and bandwidth of input RF signal, a 7-tone RF signal with central frequency of 2.95 GHz and bandwidth of 18 MHz generated by a vector signal generator (R&S SMBV100A) is also used to measure the linearity performance of APL. Due to fact that the nonlinear coefficients of transfer function are relative to the amplitude of input RF signal, the input RF power is scanned from 0 dBm to 14 dBm to vary the parameters of APL links in our experiment. The measured power ratio improvement of fundamental signal to nonlinear distortion components defined as R_{IMDs} in terms of different input RF power is shown in Fig. 10(a). The measured value of R_{IMDs} improvement is relatively low due to the tiny nonlinear distortion components when the input RF power below

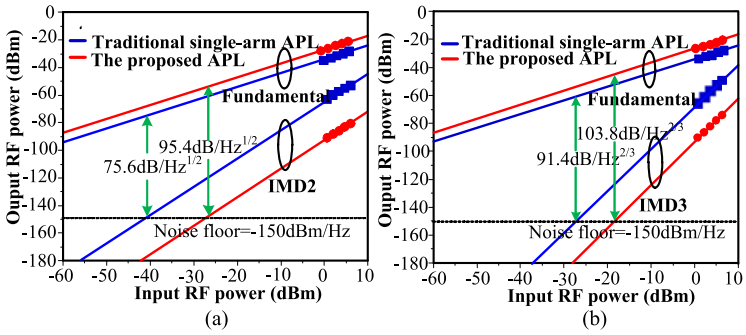

Fig. 11. Measured SFDR2 (a) and SFDR3 (b) of the traditional single-arm APL and the APL with the proposed scheme.

5 dBm. The experimental results show that the proposed DSP algorithm is effective to eliminate the nonlinear distortion components under different input RF power. As shown in Fig. 10(b) and (c), it could be clearly observed that R_{IMDs} improvement is increased by 30 dB from 26 dB to 56 dB by using the proposed DSP algorithm when the input RF power is 13 dBm. Based on the above analysis, we can draw a conclusion that the proposed DSP algorithm is effective in different situations and only bandwidth and central frequency of the input RF signal rather than modulation format, input RF power or other parameters of the APLs are required to know beforehand.

Furthermore, a two-tone signal with the central frequencies of 2.99 GHz and 3.01 GHz are generated by a vector signal generator (R&S SMBV100A) and used to test the SFDR performance of APLs. By scanning the input RF power, the powers of IMD2, IMD3 and fundamental components are monitored to measure the SFDR2 and SFDR3 of the traditional APL and the APL using the proposed scheme. The noise floor, which is dominated by the relative intensity noise of the LDs, is -150 dBm/Hz. As shown in Fig. 11(a) and (b), the SFDR2 is improved from 75.6 to 95.4 dB/Hz$^{1/2}$ and the SFDR3 is improved from 91.4 to 103.8 dB/Hz$^{2/3}$. As a result, by using the corporation of push-pull APL and the adaptive DSP algorithm, the SFDR2 and SFDR3 have been enhanced by 19.8 dB and 12.4 dB respectively, compared with the conventional single-arm APL. It indicates that both the IMD2 and the IMD3 are eliminated perfectly, and the proposed APL can be used in high linearity multi-octave applications.

5. Conclusion

In summary, to realize a broadband and high linearity directly-modulated APL, we have theoretically analyzed and experimentally demonstrated a novel nonlinearity compensation technique based on the corporation of push-pull structure and an adaptive DSP compensation algorithm. The proposed scheme could simultaneously eliminate the IMD2, HD2, IMD3, and XMD. Experimental results show that the EVM performance has been improved by 7.15% when the input RF power is 13 dBm, and the SFDR2 and SFDR3 have been improved by 19.8 dB and 12.4 dB, respectively. These results have potential applications in guiding low-cost and high-linearity optical transceiver design to realize high performance radio over fiber transmission systems and some large arrays structures.

References

[1] C. H. Cox, *Analog Optical Links: Theory and Practice*. Cambridge, U.K.: Cambridge Univ. Press, 2004.
[2] J. Capmany and D. Novak, "Microwave photonics combines two worlds," *Nat. Photon.*, vol. 1, no. 6, pp. 319–330, Jun. 2007.
[3] J. Yao, "Microwave photonics," *J. Lightw. Technol.*, vol. 27, no. 3, pp. 314–335, Feb. 2009.
[4] A. Agarwal, T. Banwell, and T. K. Woodward, "Optically filtered microwave photonic links for RF signal processing applications," *J. Lightw. Technol.*, vol. 29, no. 16, pp. 2394–2401, Aug. 2011.

[5] G. S. D. Gordon, M. J. Chisp, R. V. Penty, and I. H. White, "High-order distortion in directly modulated semiconductor lasers in high-loss analog optical links with large RF dynamic range," *J. Lightw. Technol.*, vol. 29, no. 23, pp. 3577–3586, Dec. 2011.
[6] S. Li, X. Zheng, H. Zhang, and B. Zhou, "High linear radio-over-fiber system incorporating a single-drive dual-parallel mach-zehnder modulator," *IEEE Photon. Technol. Lett.*, vol. 22, no. 24, pp. 1775–1777, Dec. 2010.
[7] T. L. Guennec, G. Maury, J. P. Yao, and B. Cabon, "New optical microwave up-conversion solution in radio-over-fiber networks for 60-GHz wireless applications," *J. Lightw. Technol.*, vol. 24, no. 3, pp. 1277–1282, Mar. 2006.
[8] R. Zhu and X. Zhang, "Broadband predistortion circuit design for electro-absorption modulator in radio over fiber system," in *Proc. 2014 Int. Conf. Opt. Fiber Commun.*, Mar. 2014, Paper W2A. 10.
[9] C. Han, S. Cho, H. Chung, and J. H. Lee, "Linearity improvement of directly-modulated multi-IF-over-fiber LTE-A mobile fronthaul link using shunt diode predistorter," in *Proc. Eur. Conf. Opt. Commun.*, Sep. 2015, Paper 0781.
[10] G. Zhang, X. Zheng, S. Li, H. Zhang, and B. Zhou, "Postcompensation for nonlinearity of Mach-Zehnder modulator in radio-over-fiber system based on second-order optical sideband processing," *Opt. Lett.*, vol. 37, no. 5, pp. 806–808, Mar. 2012.
[11] Y. Cui *et al.*, "Intermodulation distortion suppression for intensity-modulated analog fiber-optic link incorporating optical carrier band processing," *Opt. Exp.*, vol. 21, no. 20, pp. 23433–23440, Oct. 2013.
[12] Y. Cui *et al.*, "Enhanced spurious-free dynamic range in intensity-modulated analog photonic link using digital postprocessing," *IEEE Photon. J.*, vol. 6, no. 2, Apr. 2014, Art. no. 7900608.
[13] Z. Zhu, S. Zhao, X. Li, K. Qu, T. Lin, and B. Lin, "Dynamic range improvement for an analog photonic link using an integrated electro-optic dual-polarization modulator," *IEEE Photon. J.*, vol. 8, no. 2, Apr. 2016, Art. no. 7903410.
[14] V. J. Urick, J. F. Diehl, M. N. Draa, J. D. McKinney, and K. J. Williams, "Wideband analog photonic links: Some performance limits and considerations for multi-octave implementations," *Proc. SPIE*, vol. 8259, pp. 1–14, Jan. 2012.
[15] W. K. Burns, G. K. Gopalakrishnan, and R. P. Moeller, "Multi-octave operation of low-biased modulators by balanced detection," *IEEE Photon. Technol. Lett.*, vol. 8, no. 1, pp. 130–132, Jan. 1996.
[16] A. S. Hastings *et al.*, "Suppression of even-order photodiode nonlinearities in multioctave photonic links," *J. Lightw. Technol.*, vol. 26, no. 15, pp. 2557–2562, Aug. 2008.
[17] M. N. Hutchinson *et al.*, "Mitigation of photodiode induced even-order distortion in photonic links with predistortion modulation," *J. Lightw. Technol.*, vol. 32, no. 20, pp. 3885–3892, Oct. 2014.
[18] V. J. Urick, M. N. Hutchinson, J. M. Singley, J. D. McKinney, and K. J. Williams, "Suppression of even-order photodiode distortions via predistortion linearization with a bias-shifted Mach-Zehnder modulator," *Opt. Exp.*, vol. 21, no. 12, pp. 14368–14376, Jun. 2013.
[19] M. N. Hutchinson, S. R. Harmon, V. Urick, and K. J. Williams, "Analysis of magnitude and relative phase of photodiode IMD2 using amplitude matched MZM-distortion cancellation technique," *Opt. Exp.*, vol. 22, no. 1, pp. 962–971, Jan. 2014.
[20] D. Zhu, J. Chen, and S. Pan, "Multi-octave linearized analog photonic link based on a polarization-multiplexing dual-parallel Mach-Zehnder modulator," *Opt. Exp.*, vol. 24, no. 20, pp. 11009–11016, May 2016.
[21] J. Yuan, J. Wei, and G. X. Shen, "A 4-channel coil array interconnection by analog direct modulation optical link for1.5-T MRI," *IEEE Trans. Med. Imaging*, vol. 27, no. 10, pp. 1432–1438, Oct. 2008.
[22] D. Che, F. Yuan, Q. Hu, and W. Shieh, "Frequency chirp supported complex modulation of directly modulated lasers," *J. Lightw. Technol.*, vol. 34, no. 8, pp. 1831–1836, Apr. 2016.
[23] D. Marpaung, C. Roeloffzen, and W. Etten, "A broadband high dynamic range analog photonic link using push-pull directly-modulated semiconductor lasers," in *Proc. MTT-S Int. IEEE Microw. Symp.*, Jun. 2008, pp. 507–510.
[24] Y. Yao *et al.*, "A broadband and high linearity directly-modulated analog photonic link based on push-pull structure and digital signal post-compensation," in *Proc. Conf. Opt. Fiber Commun.*, Mar. 2016, Paper Th2A. 22.